ULTIMATE ASEISMIC SAFETY OF REINFORCED CONCRETE STRUCTURES

by

M. Yamada[I] and H. Kawamura[II]

SUMMARY

An analytical evaluation method for the ultimate aseismic safety of reinforced concrete structures is presented on the basis of the trapezoidal approximation of earthquake motion spectrum (Fig.2), the finite resonance principle (Figs.3,4) and the characteristics of hysteresis area (Figs.9,15) and fatigue fracture criteria (Fig.13) of R/C structures composed of flexural yielding columns and shear walls. Finally response displacement amplitudes, duration until fracture (Fig.19) and critical earthquake magnitude - epicentral distance relations (Fig.18) are calculated, by which the ultimate aseismic safety of R/C structures are clarified comprehensively and visibly.

INTRODUCTION

In earthquake structural engineering, earthquake motions, structural responses and behaviors until fracture of structures under earthquake loading should be discussed with the same accuracy. The purposes of this research are to formulate simply such succeeding mechanical behaviors on the basis of resonant response and to present an evaluation method for the ultimate aseismic safety of reinforced concrete (R/C) structures. The authors have already proposed an ultimate aseismic design method based on the behaviors of R/C structures under monotonic loading [1,2]. This report is their extended research in which cyclic and fatigue characteristics of R/C structures [3,4,5,6] are taken into account. In order to simplify and clarify the discussion on ultimate aseismic safety, R/C structures are divided into two extreme types, i.e., LC Type composed only of flexural yielding columns and SW Type only of shear walls with shear collapse mode [6]. The example of calculations is performed about these two extreme cases.

EARTHQUAKE GROUND MOTIONS

Fault Model of Earthquake Hypocenter

According to the dislocation theory, the mechanism of earthquake hypocenter is idealized as a fault model such as shown in Fig.1. In this research fundamental fault parameters are fault length L, dislocation U, rupture velocity $\bar{v}$ and dislocation velocity $\dot{u}$. From these parameters the effective duration of earthquake motions t_0 and the predominant period T_m of these earthquake waves are derived as follows:

$$t_0 = L/\bar{v} , \qquad -(1) \qquad T_m = (U/2)/\dot{u}/2 , \qquad -(2)$$

in which rise time function is assumed to be sinusoidal and so T_m becomes a half of rise time $(U/2)/\dot{u}$ [13]. When the earthquake of magnitude is evaluated as M, generally L and U depend on M but $\bar{v}$ and $\dot{u}$ do not, though

I Professor Dr.-Ing., Department of Architecture, Faculty of Engineering, Kobe University, Kobe, Japan

II Research Associate Dr.-Ing., Department of Architecture, Faculty of Engineering, Kobe University, Kobe, Japan

all of them depend on the mechanical characteristics of the crust in which the fault occurs. As for a certain seismic zone t_0 [7] and T_m [8] as well as L [9] and U [10] are expressed by exponential functions of M as follows:

$$\log t_0 = a M + b , \quad -(3) \qquad \log T_m = c M + d , \quad -(4)$$

where a, b, c and d are constants and log is the common logarithm.

Approximation of Earthquake Ground Motions

In this report spectral characteristics of earthquake ground motions are approximated to be trapezoidal as shown in Fig.2, where coordinate axes v, T_0 and t are velocity amplitude, period and time in logarithmic scale, respectively. T_G and T_m are corner periods and T_G is predominant period of surface ground (see Fig.1). α and z are acceleration and displacement amplitudes and α_0, v_0 and z_0 are constant values corresponding to α, v and z, respectively. Fig.2 shows that earthquake ground motions are stationary and random waves continuing until $t = t_0$.

Determination of α_0, v_0, z_0

In the determination of α_0, v_0 and z_0, the following assumptions are employed: (1) The relation among M, Δ(in km) and the maximum displacement amplitude Z(in cm) is given by Tsuboi's formula [11],

$$M = 1.73 \log \Delta + \log Z - 3.17, \quad -(5)$$

which is used for calculating M of earthquakes in or near Japan. (2) Z in Eq.5 is the one observed on the ground with the average T_G, i.e., 0.3 sec in Japan [12,13]. (3) Z is proportional to T_G [12,13]. (4) z_0 in Fig.2 is equal to Z. Consequently z_0, v_0, α_0 in Fig.2 are expressed by the functions of M, Δ, T_G as follows [13]:

$$\log z_0 = M - 1.73 \log \Delta - 3.17 + \log (T_G/0.3) , \quad -(6)$$

$$\log v_0 = (1 - c)M - 1.73 \log \Delta - d + \log T_G - 1.85 , \quad -(7)$$

$$\log \alpha_0 = (1 - c)M - 1.73 \log \Delta - d - 1.05 . \quad -(8)$$

FINITE RESONANT RESPONSE

Finite Resonance Principle [14]

When a one degree of freedom system with m, h, ω_j is subjected to stationary and random earthquake waves $z = \Sigma z_i \sin(\omega_i t + \phi_i)$ (see Fig.3), the system will vibrate by selecting the waves with the same circular frequency as its own ω_j from ω_i and become resonant. However, there must be a critical resonant duration t_w and number of resonant waves N_w within t_0 because of the imperfect randomness of earthquake waves. From these considerations " Finite Resonance Principle " is induced as a hypothesis in this paper as follows: (1) Input earthquake motion is $z = z_j \sin(\omega_j t + \phi_j)$. -(9) (2) There is an effective number of resonant waves N_w. (3) By reference to Housner's average response spectra [15], N_w is given as a function of viscous damping coefficient h, i.e., $N_w = 1.5\{0.5/(1 + 20h) + 0.5\}$.-(10) According to this principle, the resonant response spectrum of this system is able to be given by multiplying α_0-v_0-z_0 input spectrum by resonant amplification factor β as shown in Fig.4, where

$$\beta = \frac{1}{2h}\{1 - e^{-3\pi h(\frac{0.5}{1 + 20h} + 0.5)}\} . \quad -(11)$$

The solid lines in Fig.5 show the response spectra S_{vh} of El Centro, May 18, 1940 (NS) computed by Veletsos and Newmark [16] and the broken lines show resonant response ones based on " Finite Resonance Principle ", where S_{v0} = 122 cm/sec is assumed and $S_{v0.453} = S_{v0}/1.5\pi$ corresponds to v_0 of El Centro, May 18, 1940 (NS), because $\beta = 1$ when h = 0.453 and $\beta = 1.5\pi$ when h = 0.

Finite Resonance Response Equation for Hysteretic Systems

Based on " Finite Resonance Principle " and the following approximations: (1) Replacement of Eq.11 by $\beta = 0.6\pi/(\pi h + 0.4)$, —(12) (see Fig.6), (2) Definition of equivalent viscous damping coefficient h_e and natural period T_e in hysteretic systems shown by

$$(h =)\ h_e = A/2\pi Q_a x_a\ , \qquad -(13) \qquad (T =)\ T_e = 2\pi\sqrt{m x_a/Q_a}\ , \qquad -(14)$$

where A, Q_a, x_a and m are hysteretic area, loading amplitude, displacement amplitude and mass, respectively (see Fig.7), finite resonant response equations for hysteretic systems are able to be derived as follows:

$$\Sigma t_e \leq t_0 \qquad -(15)$$

$$T_e \leq T_G : C'_{RA} = (1/1.2\pi)(A/x_a) + 0.212\, Q_a = m\,\alpha_0\ (=\text{const.}), \qquad -(16)$$

$$T_G \leq T_e \leq T_m : C'_{RV} = (1/1.2\pi)(A/\sqrt{Q_a x_a}) + 0.212\sqrt{Q_a x_a} = \sqrt{m}\, v_0\ (=\text{const.}), \qquad -(17)$$

$$T_m \leq T_e : C'_{RD} = (1/1.2\pi)(A/Q_a) + 0.212\, x_a = z_0\ (=\text{const.}). \qquad -(18)$$

C'_{RA}, C'_{RV}, and C'_{RD} are named here finite resonance acceleration, velocity and displacement capacities, respectively.

HYSTERETIC ENERGY ABSORPTION AND FATIGUE FRACTURE CRITERIA OF R/C STRUCTURES

R/C Columns with Flexural Yielding Type (LC Type)

Consider a R/C column with flexural yielding type subjected to alternately repeated story shear force Q and constant axial load N which is smaller than the balancing level (see Fig.8), then its hysteresis loop of shear force Q and lateral displacement x with displacement amplitude x_a is idealized as shown by thick lines in Fig.9, where Q_y is yielding Q, Q_s slipping Q and x_y yielding x [4]. The thin solid line hysteresis loop is the one in which Bauschinger's effect is neglected. The hysteresis loop of moment M - curvature Φ with curvature amplitude Φ_a in Fig.10, where the suffixes y, s of M mean the same as of Q, is used to calculate this Q - x relation. This M - Φ loop is derived from the R/C cross section, strain distribution and stress distribution in Fig.11. The Roman numerals (I), (II) (III) in Figs.10,11 correspond to the mechanical states, i.e., flexural yielding, starting of slip and end of slip, respectively. Based on Figs. 8,11 the critical values M_y, Φ_y, Q_y, x_y, M_s and Q_s in Figs.9,10 are given as follows:

$$M_y/F_c bD^2 = \frac{1}{2}(1 - x_{n_1})x_{n_1} + \beta_s p(1 - 2d_1)\ , \qquad -(19) \qquad D\Phi_y = 2\varepsilon_y/(1 - 2d_1), \qquad -(20)$$

$$Q_y/F_c bD = 2(M_y/F_c bD^2)/(H/D), \qquad -(21) \qquad x_y = \frac{1}{6}D\Phi_y(H/D)H, \qquad -(22)$$

$$M_s/F_c bD^2 = (2\beta_s p - x_{n_1})(1 - 2d_1)/2, \qquad -(23) \qquad Q_s/F_c bD = 2(M_s/F_c bD^2)/(H/D), \qquad -(24)$$

where $x_{n_1} = N/F_c bD$, —(25) $\beta_s p = (\sigma_y/F_c)/(a/bD)$, —(26)

Then hysteresis loop area A is reduced to $A = \frac{1}{4}(5Q_y + 9Q_s)(x_a - x_y)$. —(27)

The strength of compressive concrete block F_c in Fig.11-c is deteriorated by repetition of loading. The effect of number of cycles N_c on deterioration factor $\gamma (= F_c(N_c)/F_c)$ is assumed here to be (see Fig.12)

$$\gamma = 1 - (1/8)\log N_c \qquad -(28)$$

Assuming that fatigue fracture occurs when the compressive strain in compressive reinforcing bar reaches the ultimate compressive strain of concrete ${}_c\varepsilon_B$ and that ${}_c\varepsilon_B = 4 \times 10^{-3}$, the relation between curvature amplitude Φ_a and number of cycles to fracture N_B is reduced to

$$D\Phi_a = 4 \times 10^{-3}/\{x_{n_1}/(1 - \tfrac{1}{8}\log N_B) - d_1\} , \qquad -(29)$$

and the displacement amplitude x_a at that time is given by

$$x_a = x_y + H\tfrac{1}{2}D(\Phi_a - \Phi_y) , \qquad -(30)$$

where plastic hinge method is used and longitudinal length of plastic hinge is assumed to be (1/2)D.

R/C Shear Walls (SW Type)

Relationship between story shear force Q and lateral displacement x of R/C shear walls under cyclic Q shown in Fig.14 is idealized as shown in Fig. 15, where Q_B and x_B are the ultimate shear capacity and displacement, respectively, the suffix i shows ordinal number of cycles [5]. Through the idealization of concrete shear panel into equivalent diagonal compressive brace (see Fig.14), Q_B and x_B are calculated as follows:

$$Q_B = \tfrac{1}{2} F_c Lt \sin\theta \cos\theta , \quad -(31) \qquad x_B = 2 \times 10^{-3} L/\cos^2\theta . \quad -(32)$$

Considering the slipping and overlapping characteristics of hysteresis loops of R/C shear walls, hysteresis loop area A_i is approximately given by the function of x_i, x_{i-1}, x_{i-2} as follows:

for i near to the unity; $A_i/Q_B x_B = (x_i/x_B)^2 - \frac{1}{2}(x_{i-1}/x_B)^2$, $\quad -(33)$

for larger i ; $A_i/Q_B x_B = (x_i/x_B)^2 - (x_{i-2}/x_B)^2$. $\quad -(34)$

Fracture criterion of R/C shear walls is $x_a = x_B$. $\quad -(35)$

The fatigue criteria of R/C columns of flexural yielding type (LC Type) [17] and R/C shear walls (SW Type) are shown in the $\log x_a - \log N_B$ plane in Fig.13.

ULTIMATE ASEISMIC SAFETY OF R/C STRUCTURES

Analytical Procedures and Calculation Results

When M, Δ and T_e are given, α_0, v_0, z_0 are derived from Eqs.3,6,7,8. As for LC Type, substituting A in Eq.27 into Eqs.16,17 or 18, x_a is solved and response number of cycles n_0 during t_0 is derived from Eq.14 and $Q_a = Q_y$ as

$$n_0 = t_0/T_e \qquad -(36)$$

On the other hand N_B is computed by Eqs.29,30 and the ultimate aseismic safety of LC Type is estimated by the comparison between response number n_0 and N_B. As for SW Type, substituting A_i in Eqs.33 or 34 into Eqs.16,17 or 18, x_a is given as a solution of difference equation, i.e., a function of i, and from Eq.36 response displacement amplitude x_{an0} is obtained. The ultimate aseismic safety of SW Type is estimated by the comparison between x_{an0} and x_B. When M and Δ are unknown, we can calculate a critical $M_{cr} - \Delta_{cr}$ relation in which $n_0 = N_B$ for LC Type and $x_{an0} = x_B$ for SW Type. Against earthquake motions with the smaller M and larger Δ than this $M_{cr} - \Delta_{cr}$ curve structures never collapse, and vice versa. For calculation examples the LC and SW Types shown in Figs.16,17 are employed. The calculation conditions are as follows: strength of concrete $F_c = 210$ kg/cm^2, yield strength of steel ${}_s\sigma_y = 3{,}500$ kg/cm^2, yield strain of steel ${}_s\varepsilon_y = 1.75 \times 10^{-3}$. For SW Type , seismic weight W (= axial load N) = 120 tons, yield shear coefficient

k_y (= Q_y or Q_B/W) = 0.275. For LC Type, W = 1833, 916, 458 tons, k_y = 1,100, 0,550, 0,275. Fig.18 shows the critical M_{cr} - Δ_{cr} curves with numbers of cycles to fracture, where the constants in Eqs.3,4 are assumed as a = 0.5, b = -2.28, c = 0.5, d = -2.91. The one dotted line shows the minimum Δ_{min} curve calculated under the conditions that

$$z_0 \leq U/4, \qquad -(37) \qquad \log U = 0.55M - 3.71 \ [10], \qquad -(38)$$

and T_G = 0.3 sec. In the region $\Delta \geq \Delta_{min}$ the M_{cr} - Δ_{cr} relations are effective. Fig.19 shows the processes of the resonant response displacement x_a and duration ΣT_e until fracture of LC Type (k_y = 0.275) and SW Type (k_y = 0.55) under the critical earthquake motions with M_{cr} - Δ_{cr}.

Estimation of Ultimate Aseismic Safety

The x-marks in Fig.18 show the actual earthquake motions in Japan. We can derive direct informations on the ultimate aseismic safety of R/C structures from the comparison between x-marks and M_{cr} - Δ_{cr} relations. If M and Δ are given by a probability density function $f(M,\Delta)$ within a time interval, a probability of fracture p_B is able to be calculated as follows:

$$p_B = \int_\Omega f(M,\Delta)\, dM\, d\Delta \ , \quad \text{(see Fig.20)} \qquad -(39)$$

where Ω is a fracture region which is shown in Fig.21.

CONCLUSIONS

In this report analytical procedures and calculation results for the ultimate aseismic safety of R/C structures are presented. If critical earthquake magnitude M_{cr} - hypocentral distance Δ_{cr} relations are obtained reasonably, ultimate aseismic safety will be estimated by a deterministic or probabilistic value, which is effective not only for R/C structures but also for all types of structures.

REFERENCES

[1] Yamada,M.,Kawamura,H.; Proc., 5WCEE, Rome, 1974, Vol.1, pp.864-867.
[2] Yamada,M.,Kawamura,H.; Proc., 6WCEE, New Delhi, 1977, Vol.1, pp.197-202.
[3] Yamada,M.,Kawamura,H.; ACI Publication SP-53, 1977, pp.81-108.
[4] Yamada,M.,Kawamura,H.; Prel. Rep., IABSE Symp., Lisboa,1973, pp.199-204.
[5] Yamada,M.,Kawamura,H.; Proc., 6WCEE, New Delhi,1977,Vol.III,pp.3075-80.
[6] Yamada,M.,Kawamura,H.; Proc., 6WCEE, New Delhi,1977,Vol.II, pp.1835-40.
[7] Gutenberg,B.,Richter,C.F.; Bull.,Seism. Soc. America, Vol.46, 1956, pp. 105-145.
[8] Kasahara,K.; Bull.,Earthq.Res.Inst.,Tokyo Univ.,Vol.35,1957,pp.473-532.
[9] Otsuka,M.; Zishin (Journl.,Seism. Soc. Japan) ii,18, 1965, pp.1-8.
[10] Iida,K.; Journl.,Earth. Sciences, Nagoya Univ., Japan, Vol.13,No.2,1965, pp.115-132.
[11] Tsuboi,C.; Zishin (Journl.,Seism. Soc. Japan) ii,Vol.7,No.3, 1964, pp. 185-193.
[12] Seism. Div.; Japanese Meteor. Admin.; Quat. Journl. Seism., J.M.A.,Vol. 37, No.3, 1972, pp.113-115.
[13] Yamada,M.,Kawamura,H.; Trans.Arch.Inst.Japan,No.279,May 1979,pp.29-40.
[14] Yamada,M.,Kawamura,H.; Trans.Arch.Inst.Japan,No.287,Jan.1980,pp.68-76.
[15] Housner,G.W.; Proc., 1WCEE, Berkeley, 1956, pp.5-1-5-13.
[16] Veletsos,A.S.,Newmark,N.M.; Proc., 2WCEE, Tokyo-Kyoto,1960, pp.895-912.
[17] Yamada,M.,Kawamura,H.,Furui,S.; RILEM Internl.Symp.Mexico,Vol.6,1966, pp.1-13

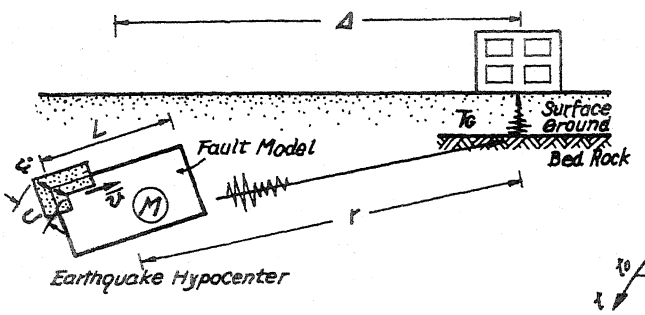

Fig.1 Path of Earthquake Waves From the Hypocenter to a Structure

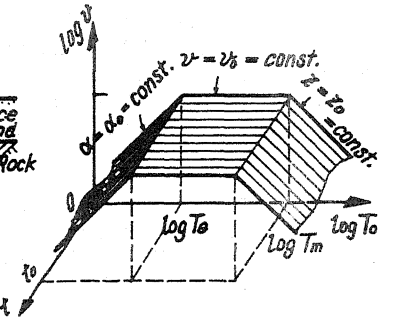

Fig.2 Idealized Spectrum of Earthquke Ground Motions

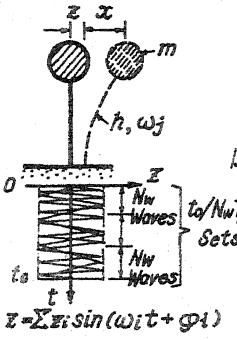

Fig.3 One Degree of Freedom System

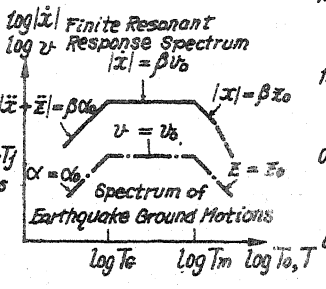

Fig.4 Response Spectrum by "Finite Resonance Principle"

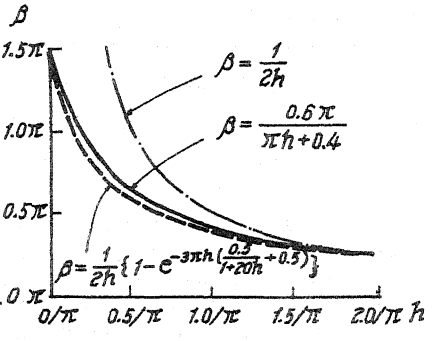

Fig.6 Approximation of Finite Resonant Response Amplification Factor β

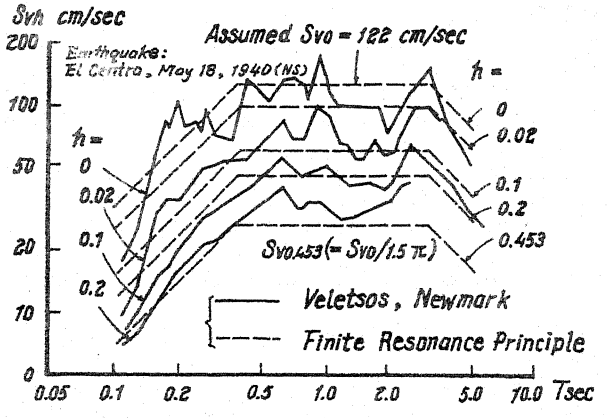

Fig.5 Comparison Between Numerically Integrated Response Spectra and Finite Resonance Spectra

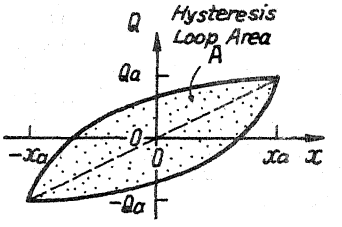

Fig.7 Equivalent Viscous Damping Coefficient h_e and Natural Period T_e

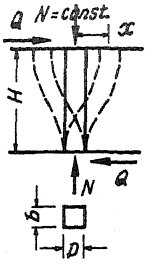

Fig.8 R/C Column

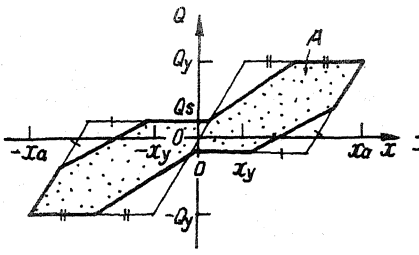

Fig.9 Shear Force Q - Lateral Displacement x Relation of R/C Column

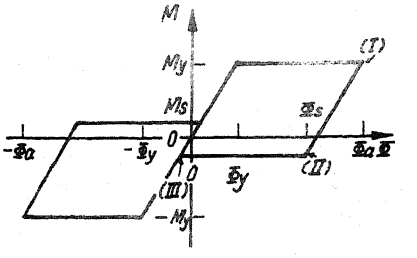

Fig.10 Moment M - Curvature Φ Relation of R/C Column Cross Section

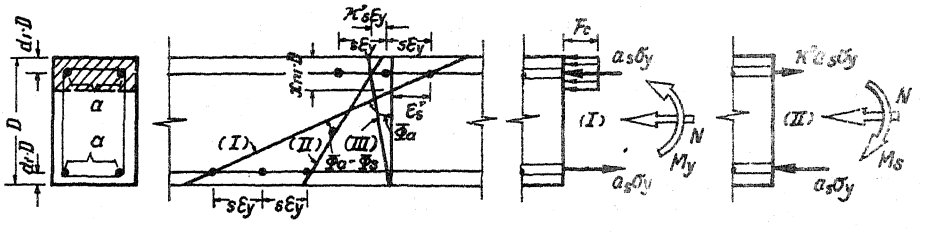

(a) Cross Section (b) Strain Distribution (c) (I) Stress Distribution (d) (II) Stress Distribution

Fig.11 Cross Section, Strain and Stress Distributions of R/C Column

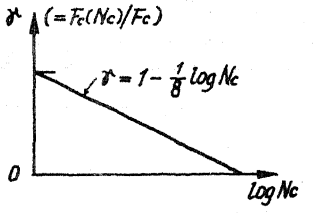

Fig.12 Deterioration Factor γ - Number of Cycles N_c Relation

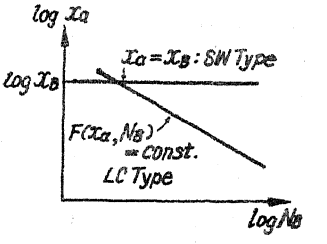

Fig.13 Fracture Criteria of R/C Columns (LC Type) and R/C Shear Walls (SW Type)

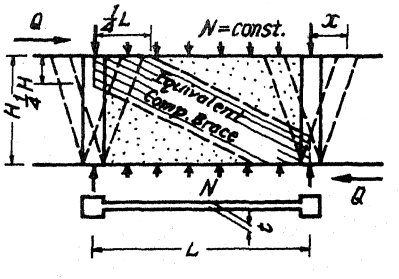

Fig.14 R/C Shear Wall

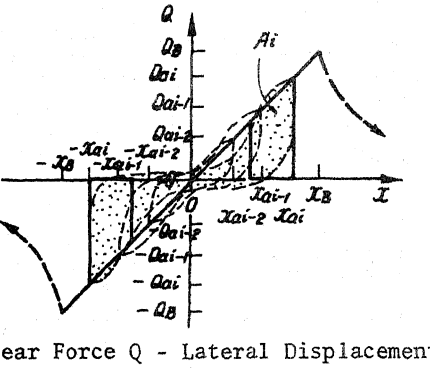

Fig.15 Shear Force Q - Lateral Displacement x Relations of R/C Shear wall

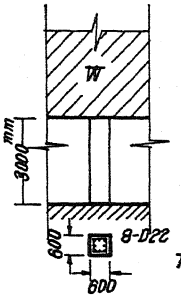

Fig.16
Assumed R/C
Column

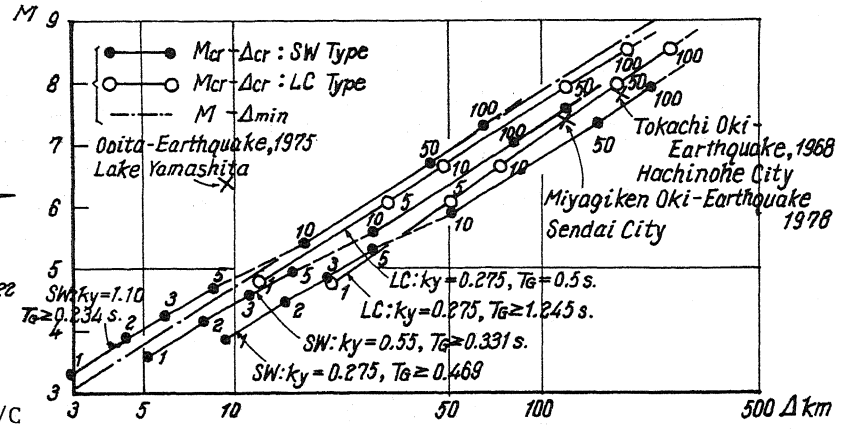

Fig.18 Critical Earthquke Magnitude M_{cr} - Hypocentral Distance Δ_{cr} Relations of R/C Structures

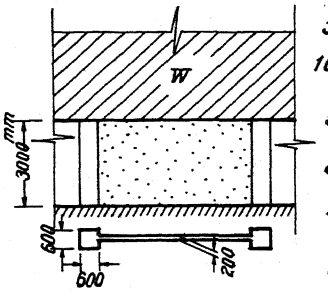

Fig.17 Assumed R/C
Shear Wall

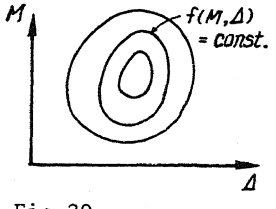

Fig.20
Probability Density
Function of M and Δ

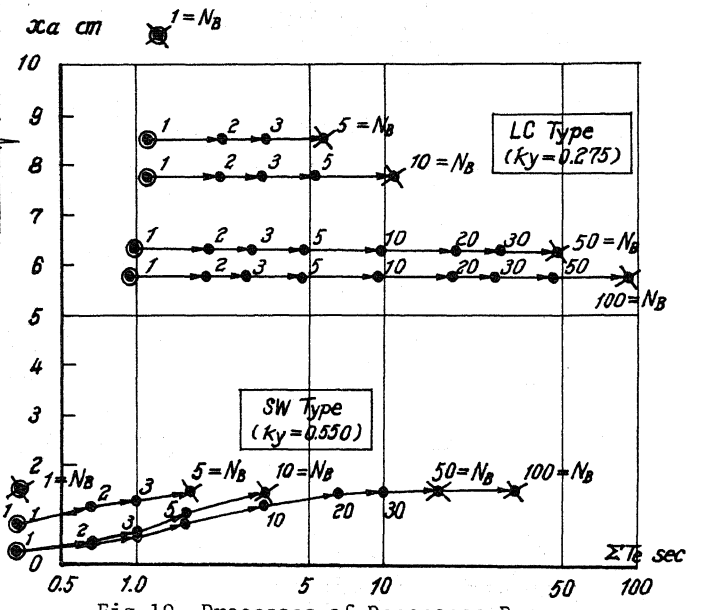

Fig.19 Processes of Resonance Response Displacement and Duration Until Fracture of R/C Structures

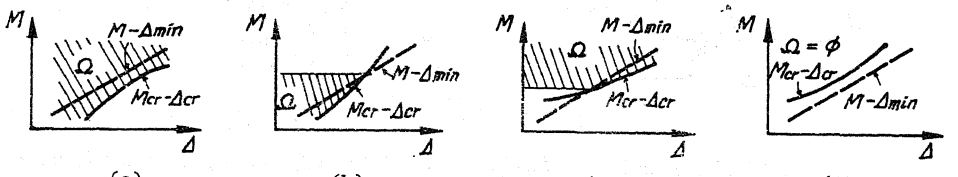

Fig.21 Fracture Region Ω of M and Δ